

Learning to Generate Rigid Body Interactions with Video Diffusion Models

David Romero¹, Ariana Bermudez¹, Hao Li^{1,2}, Fabio Pizzati¹, Ivan Laptev¹
¹MBZUAI, UAE ²Pinscreen, USA

{david.romero, ariana.venegas, hao.li, fabio.pizzati, ivan.laptev}@mbzuai.ac.ae



Figure 1. **KineMask results.** We enable object-based control with a novel training strategy. Paired with synthetic data constructed for the task, KineMask enables pretrained diffusion models to synthesize realistic rigid body interactions in real-world input scenes.

Abstract

Recent video generation models have achieved remarkable progress and are now deployed in film, social media production, and advertising. Beyond their creative potential, such models also hold promise as world simulators for robotics and embodied decision making. Despite strong advances, however, current approaches still struggle to generate physically plausible object interactions and lack object-level control mechanisms. To address these limitations, we introduce KineMask, an approach for video generation that enables realistic rigid body control, interactions, and effects. Given a single image and a specified object velocity, our method generates videos with inferred motions and future object interactions. We propose a two-stage training strategy that gradually removes future motion supervision via object masks. Using this strategy we train video diffusion models (VDMs) on synthetic scenes of simple interactions and demonstrate significant improvements of rigid body interactions in real scenes. Furthermore, KineMask integrates low-level motion control with high-level textual conditioning via predicted scene descriptions, leading to support for synthesis of complex dynamical phenomena. Our experiments show that KineMask achieves strong improvements over recent models of comparable size. Ablation studies further highlight the complementary roles of low- and high-level conditioning in VDMs. Project Page: <https://daromog.github.io/KineMask/>

1. Introduction

Recent years have seen substantial advances in video generation, with Video Diffusion Models (VDMs) emerging as a leading paradigm for high-resolution, temporally consistent synthesis [10, 25, 31, 61]. This progress has elevated visual quality and enabled early commercial use in creative performances [40], experimental filmmaking [12], and advertising [47]. Beyond content creation, VDMs have also been explored as world models [23], capable of anticipating real-world interactions and supporting robotics and embodied decision making [3, 5, 18]. Realizing this vision, however, requires strict physical plausibility and control, since small deviations from realistic physics can accumulate into large errors in predicted dynamics. Yet, current VDMs struggle to capture fundamental traits [30, 41] such as object permanence, collisions and causal interactions, even for large-scale models like Veo-3 [60]. Hence, methods for physically accurate video generation are a key step toward establishing VDMs as reliable world models. Recent frameworks such as WonderPlay [37], PhysGen [39] and PhysGen3D [13] integrate physics-based simulators into data-driven video generation, but rely on explicit scene reconstruction, a challenging task on its own. Differently, drag-based approaches [15, 19, 32, 35, 50, 66, 68] can move objects, but often requiring pre-defined target points, thus preventing the inference of causal effects of motion from starting conditions only. Around the time of this work, Force Prompting [20] introduced physics-guided

controls into VDMs using simulated training data. While promising, it offers limited fine-grained control and object interactions realism, often producing unrealistic dynamics, and distorted shapes, showing a lack of understanding of causality. Motivated by these limitations, we propose an approach enabling video diffusion models to generate physically realistic object interactions, as a core requirement for robotics and video generation. Our approach aims to answer two central questions for world models: **(1)** Can a video diffusion model generate *realistic interactions* between rigid bodies given initial dynamic conditions, and **(2)** how do data and textual conditioning influence the emergence of causal physical effects in generated videos?

To address these questions, we introduce KineMask, a framework for generating accurate object interactions and effects in complex scenes (Figure 1). KineMask provides *low-level* kinematic control over parameters such as object direction and speed, while *inferring object interactions directly within the VDM*. KineMask is trained on simulator-rendered videos that capture not only physically valid dynamics but also explicit object interactions, paired with textual descriptions of the underlying events. We leverage object masks as guidance, enabling single-frame motion control and improving the model’s understanding of shapes. Beyond low-level control, KineMask integrates *high-level* prompt conditioning through textual descriptions of future scene dynamics. At inference, it predicts dynamics from an input image and enables the generation of complex effects, such as liquid spilling (Figure 1). Extensive experiments show that KineMask not only introduces new control capabilities but also outperforms state-of-the-art models of comparable size, while ablation studies highlight the importance of both the proposed training strategy and the integration of low- and high-level controls.

In summary, we propose the following contributions:

- We introduce KineMask, a mechanism for object motion conditioning in VDMs, based on a novel two-stage training and conditioning encoding.
- We train KineMask on a synthetic dataset of dynamic scenes with simple object interactions and demonstrate generalization to complex interactions in real scenes.
- We combine low-level motion control with high-level text conditioning, yielding significant gains over comparable models in video synthesis of rigid body interactions.

2. Related works

Video Diffusion Models. Early video diffusion directly extended image generators by inserting temporal layers into denoising U-Nets [2, 7, 9, 14, 22, 57, 59]. Later, video synthesis improved through the usage of Diffusion Transformers (DiTs) [44], inheriting scaling properties from native transformer-based architectures. The use of DiTs allowed for higher-resolution videos and stronger

visual quality [24, 31, 55, 61]. We build KineMask on CogVideoX [61], benefiting from the advantages of DiTs. Beyond creative purposes, diffusion-based video generation is now used for *world modeling*, by synthesizing the possible outcomes of actions in an environment. [5, 54] first proposed diffusion-based world models on restricted scenarios. Some like GAIA [26, 48] train at scale on specific domains such as autonomous driving, while Cosmos [3] uses large-scale data to handle heterogeneous domains. These models still suffer from limited realism in generating object interactions, motivating our study.

Control for video generation Significant efforts have been made to extend control on generated videos beyond textual conditioning. On images, ControlNet [63] and similar approaches [42, 67] proposed plug-and-play control trainable components for dense conditioning such as edges, depth, or human poses. In videos, VideoControlNet [27] propagated conditions frame by frame using optical flow, while others focused on pose-driven human video generation [65] or keyframe-to-video propagation [34]. More recent works such as SparseCtrl [21] uses just a few keyframes for sketch, depth, or image conditioning, ignoring motion conditions. MotionI2V [49] first infers object motion with flow generation, then it renders a video using flow as control. A significant line of works allows motion control with dragging trajectories [17, 19, 32, 35, 50, 56, 62, 66, 68]. While effective, these require pre-defined trajectories, and are unable to infer motion causal effects from initial conditions. Some drive motion by directly guiding attentions [45] or noise [11] using reference videos. Beyond single modalities, Cosmos-Transfer [1] demonstrates adaptive multimodal conditioning. To our knowledge, KineMask is the first approach training VDMs to generate rigid body interactions by controlling *initial object velocity only*.

Physics-aware video generation The interactions between physical understanding and video generation is a growing research field. A first line of work integrates physical simulations with learning-based techniques. In particular, PhysDreamer [64] generates oscillatory motions on 3D Gaussians, while DreamPhysics learns physical properties of dynamic 3D Gaussians with video diffusion priors [28]. On video generation, WonderPlay [37] bridges physics solvers and generative video models to synthesize dynamic 3D scenes across diverse physical phenomena. PhysGen3D [13] and PhysGen [39] apply a similar approach using 3D and 2D information respectively for rigid body interactions. However, the use of a simulator requires significant engineering efforts and limits the flexibility of models. Differently, others [8, 16] map input kinematics to future frames, but requiring dataset-specific training. Instead, C-Drag [36] infers causal motion on output videos with LLMs, and combines it with tracking control to al-

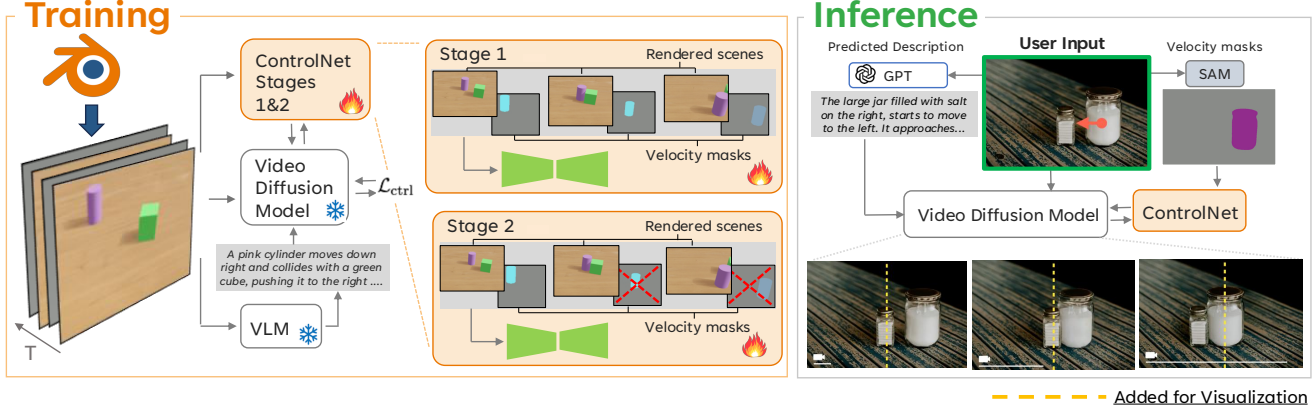


Figure 2. **KineMask pipeline.** We encode our *low-level* control signal as a mask encoding the velocity of the moving objects, to train a ControlNet (left) in two stages using Blender-generated videos of objects in motion. In the first one, we train with all frames, whereas in the second one, we randomly drop part of the final frames. We also provide a *high-level* textual control extracted by a VLM. At inference (right), we construct the low-level conditioning with SAM and use GPT to infer high-level outcomes of object motion from a single frame.

low video generation. Using purely diffusion models, InterDyn [4] explores the capability of video models to render realistic object dynamics. However, it exploits frame-wise masks of controlling elements, which are typically unavailable at test time. Similarly to us, [33] explores physics post-training but focuses on gravity effects. Force Prompting [20] explores similar ideas to ours but does not consider object interactions and deploys simpler motion control. We compare to Force Prompting and demonstrate improved performance synthesizing object interactions.

3. KineMask

KineMask is designed to synthesize realistic interactions among rigid bodies given an input image and the object velocity encoded by an object mask, as in Figure 2. Below, we introduce preliminaries in Section 3.1. We then describe our conditioning mechanism in Section 3.2 and outline the training and inference procedure in Section 3.3.

3.1. Preliminaries

Video diffusion Models. VDMs generate data by reversing the noising process. In training, a clean video $\mathbf{x}_0 \in \mathbb{R}^{F \times H \times W \times C}$ is perturbed into a noisy version \mathbf{x}_t by adding Gaussian noise at a randomly sampled timestep t , and the model is optimized to approximate the corresponding reverse transition. At inference, the process is inverted: starting from pure Gaussian noise \mathbf{x}_T , the model denoises through intermediate states $\{\mathbf{x}_t\}_{t=1}^T$ until it recovers a clean output video \mathbf{x}_0 after T steps. To be grounded to real scenes, we use image-to-video (I2V) models, where the video synthesis is conditioned on a reference image \mathbf{y} . Formally, we denote by p_θ the VDM with parameters θ . Conditioned on a high-level text description of the desired output c and a reference image \mathbf{y} , the denoising step is:

$$\mathbf{x}_{t-1} \sim p_\theta(\mathbf{x}_{t-1} | \mathbf{x}_t, c, \mathbf{y}), \quad (1)$$

where \mathbf{x}_{t-1} is a tensor defined over the frame dimensions. The training loss minimizes the KL divergence between the true reverse conditional p and the model distribution:

$$\mathcal{L}_{\text{diff}}(\theta; \mathbf{x}_0, \mathbf{y}, c, t) = D_{\text{KL}}(p(\mathbf{x}_{t-1} | \mathbf{x}_t, \mathbf{x}_0) || p_\theta(\mathbf{x}_{t-1} | \mathbf{x}_t, c, \mathbf{y})). \quad (2)$$

In practice, this objective is implemented by a noise prediction task in which the network learns to estimate the Gaussian noise added to \mathbf{x}_0 .

ControlNet. To allow additional guidance, a ControlNet [63] branch ψ_ϕ , parameterized by ϕ , can encode an arbitrary dense control signal $\mathbf{u} \in \mathbb{R}^{F \times H \times W \times D}$ driving the output generation. For more details, please refer to [63]. The denoising step then becomes:

$$\mathbf{x}_{t-1} \sim p_\theta(\mathbf{x}_{t-1} | \mathbf{x}_t, c, \mathbf{y}, \psi_\phi(\mathbf{u})). \quad (3)$$

When training the ControlNet, the parameters of the backbone model θ are kept frozen, while only the control branch ϕ is optimized. The corresponding loss is:

$$\mathcal{L}_{\text{ctrl}}(\phi; \mathbf{x}_0, \mathbf{y}, \mathbf{u}, c, t) = D_{\text{KL}}(p(\mathbf{x}_{t-1} | \mathbf{x}_t, \mathbf{x}_0) || p_\theta(\mathbf{x}_{t-1} | \mathbf{x}_t, c, \mathbf{y}, \psi_\phi(\mathbf{u}))). \quad (4)$$

3.2. Enabling motion control

First-stage training. We now want to enable object-wise motion control for KineMask. Specifically, our goal is to move an object in an input scene \mathbf{y} with controlled direction and velocity, allowing us to study the effects of object interactions in the videos generated with diffusion models. To do so, we assume access to a dataset \mathcal{D} of captioned

videos depicting objects in motion. Let $f \in \{1, \dots, F\}$ denote the frame index. For each frame f and object in the scene, we are given a mask $\mathbf{m}_f \in \mathbb{R}^{H \times W \times 3}$ aligned with the image resolution. The three channels encode the instantaneous velocity vector, with the red, green, and blue channels corresponding to motion along the x -, y -, and z -axes, respectively, in the pixels defined by a segmentation mask of the object. In this way, \mathcal{D} provides not only spatial information about object locations, but also explicit ground-truth dynamics. The velocity masks are then aggregated into a tensor $\mathbf{m} \in \mathbb{R}^{F \times H \times W \times 3}$ and used to condition ψ_ϕ . Similarly to [4], we annotate in this way only the velocity of the objects moving in the first frame of the rendered video, leaving blank the mask for objects potentially moved by interactions. We visualize our strategy in Figure 2 (top). This enforces the model to synthesize interactions without explicitly relying on pixel control. We can then train a *first-stage* KineMask ControlNet ϕ' by solving

$$\phi' = \arg \min_{\phi} \mathbb{E}_{(\mathbf{x}_0, \mathbf{y}, \mathbf{m}, c) \sim \mathcal{D}, t} \left[\mathcal{L}_{\text{ctrl}}(\phi; \mathbf{x}_0, \mathbf{y}, \mathbf{m}, c, t) \right], \quad (5)$$

The ϕ' network learns to map dense pixel-wise supervision into structured guidance for object motion in the generated videos. We show the training masks in Figure 2 (top).

Second-stage training. KineMask ϕ' enables motion control given motion masks \mathbf{m} provided for all the frames of a video. While such a setup simplifies training, it does not correspond to our desired scenario of video generation conditioned *only* by the object motion at the first video frame. Towards this goal, we use a mask dropout strategy, randomly erasing part of the velocity masks in \mathbf{m} at training time, as shown in Figure 2 (bottom). Formally, we define a truncated mask tensor

$$\mathbf{m}_\odot = \{\mathbf{m}_{\odot, f} = \mathbf{m}_f \text{ if } f \in f^*, \mathbf{0} \text{ otherwise}\}_{f=0}^F. \quad (6)$$

where f^* denotes the masked frame indices, and depends on the dropout ratio. Thus, only some frames contain velocity supervision, while the remainder of the sequence is set to zero. We then train a *second-stage* KineMask ϕ'' by finetuning ϕ' with this strategy, solving

$$\phi'' = \arg \min_{\phi''} \mathbb{E}_{(\mathbf{x}_0, \mathbf{y}, \mathbf{m}, c) \sim \mathcal{D}, t} \left[\mathcal{L}_{\text{ctrl}}(\phi'; \mathbf{x}_0, \mathbf{y}, \mathbf{m}_\odot, c, t) \right]. \quad (7)$$

As a result of the dropout during training, the VDM equipped with ϕ'' is able to move objects by taking as input only the *initial* velocity, with $\mathbf{m}_\odot = \{\mathbf{m}_0, \mathbf{0}, \dots, \mathbf{0}\}$. Ultimately, to render realistic videos, the VDM *must synthesize motion dynamics* starting from initial conditions only.

3.3. Data

Training. We show our training pipeline in Figure 2 (left). For training ϕ'' , we assumed the availability of a dataset

$\mathcal{D} = \{(\mathbf{x}_0, \mathbf{y}, \mathbf{m}, c)\}$. Besides the target video \mathbf{x}_0 and the reference conditioning image \mathbf{y} , we require both *low-level* and *high-level* conditioning for physical dynamics. At the low level, we require the aggregated velocity masks \mathbf{m} defined in Section 3.2. At the high level, instead, we associate each video with a textual description c summarizing the effects of physical interactions. Since collecting real-world videos with such annotations is impractical, we generate synthetic data in Blender. Importantly, such simulated data still allows to generalize to real scenes, as we empirically verify in our experiments. We render scenes with boxes and cylinders placed on textured surfaces, and assign to each controlled object an initial velocity with random direction and magnitude. This procedure yields \mathbf{x}_0 as the rendered video, \mathbf{y} as the first frame of the sequence (used for image-to-video conditioning), and \mathbf{m} as the stack of per-frame velocity masks, which provide supervision of motion. To obtain the high-level descriptions c , we instead process each rendered video with a vision–language model (VLM), prompted to provide detailed video captions with particular focus on object interactions. The full prompt used for caption generation is reported in Appendix A.2.

Inference. We assume as input an unseen image \mathbf{y} . An object mask is obtained for the target object e.g., using SAM2 [46], while the desired object velocity at the first frame is assumed to be provided by the user. We use this information to construct \mathbf{m}_\odot . We also prompt GPT-5 [43] for a description c_{infer} of the effects on the scene if the object starts moving in the direction indicated by the user. The full prompt is in Appendix A.2. Combining those with random noise $\mathbf{x}_T \sim \mathcal{N}(0, 1)$, we construct the input tuple $\{\mathbf{x}_T, \mathbf{y}_{\text{input}}, \mathbf{m}_\odot, c_{\text{infer}}\}$ compatible with our VDM equipped with ϕ'' . Our inference pipeline is illustrated in Figure 2 (right). Please note that at inference the user simply draws an arrow, mapped to RGB masks automatically.

4. Experiments

We describe the experimental setup in Section 4.1. Section 4.2 presents our main results and compares KineMask to the state of the art. Finally, Section 4.3 shows a comprehensive analysis with ablations for different components of our method. Further ablations are in Appendix A.3.

4.1. Setup

Datasets. We generate two datasets for training and evaluation. Following Section 3.3, we render cubes and cylinders with random colors, moving on textured backgrounds from AmbientCG [6]. The first *Interactions* dataset contains objects moving in random directions and interacting with each other. We also construct a *Simple Motion* dataset, where isolated objects are moving in random directions without



Figure 3. **Qualitative comparison with CogVideoX.** While CogVideoX often suffers from several failure modes, such as hallucinations and incorrect motions, KineMask follows target motion and generates realistic object interactions. In details, we improve object interactions in collisions (top row), show causal effects of object motion (bottom left), and move multiple objects (bottom right).

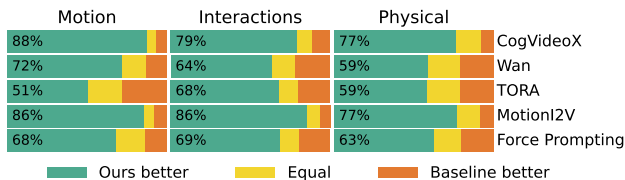


Figure 4. **User study.** We widely outperform baselines on motion fidelity, interaction quality, and overall physical consistency.

collisions. For both, we generate 10,000 training and 100 test samples. Test videos use disjoint colors and textures compared to training to ensure diversity. We visualize samples of the generated data in Appendix A.2. We also include a *Real World* set of 50 images, collected from the web or generated with ChatGPT’s image generator [29], used to assess generalization to real scenes with complex objects. Note that unlike *Simple Motion* and *Interactions*, *Real World* does not include ground-truth motion trajectories. We use Tarsier [58] to extract predictive captions c .

Implementation. We adopt CogVideoX-I2V-5B (CogVideoX) as backbone for KineMask. We use ControlNet on the first 8 layers of the model, with weight at 0.5. For ϕ'' , we also apply a non-uniform sampling strategy for f^* , where frame selection is biased toward earlier frames, as rigid body interactions occur most frequently at the beginning of the simulated sequences. Further details are provided in Appendix A.2. We generate 49 frames at inference.

Baselines. We consider two baselines using pretrained image-to-video models: CogVideoX [61] and Wan2.2-I2V-5B [55] (Wan). We prompt both baselines with the same c_{infer} as used for KineMask. Since we use CogVideoX as a backbone for KineMask, these two methods only differ by our training procedure. We choose TORA [66], also based on CogVideoX, as a drag-based baseline. Since TORA requires the full drag trajectory, we draw it starting from the target object depending on the input velocity (see Appendix A.2). We also include MotionI2V [49] as mask-constrained drag method, that we prompt using SAMv2 masks and a drag trajectory similar to TORA. Finally, we evaluate Force Prompting (FP) [20], by mapping our input velocity to input force prompts [20]. Force Prompting is also built on CogVideoX. More details are in Appendix A.2.

Metrics. For visual quality, we report the Fréchet Video Distance (FVD) [53] and the mean squared error (MSE) between generated and ground-truth videos in our synthetic test sets. For motion, we compute the Fréchet Video Motion Distance (FVMD) [38], which isolates motion quality from appearance. Finally, we use SAM2 [46] to extract semantic masks of objects in generated videos, and compute Intersection over Union (IoU) with ground-truth masks and assess geometric consistency.

4.2. Comparison with baselines

Qualitative comparison. We demonstrate qualitative improvements on *Real World* scenes. While for space rea-

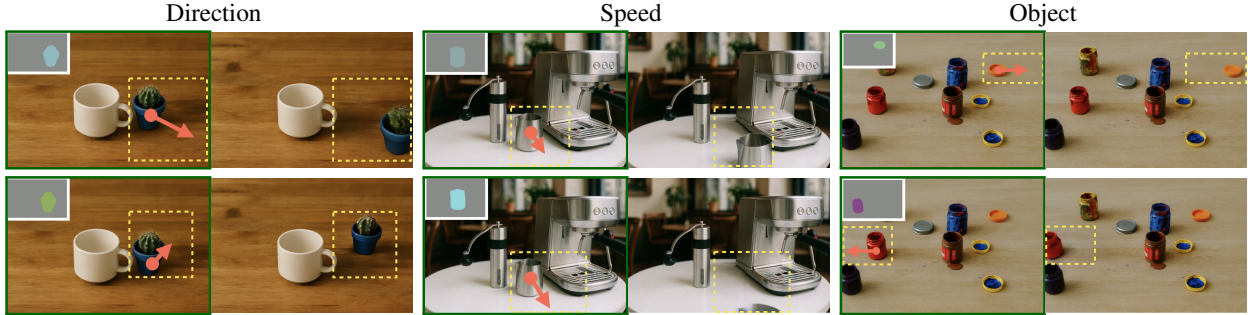


Figure 5. **Degrees of freedom.** We show control of different aspects of KineMask outputs. We can choose different directions (left), speed (middle), and objects to move (right), opening potential for world modeling.

<i>Simple Motion</i>				
Method	MSE↓	FVD↓	FMVD↓	IoU↑
CogVideoX	158.3	601.1	1504.6	0.051
2nd stage only	86.3	288.8	201.0	0.237
Ours (1st + 2nd stage)	47.2	160.3	199.8	0.367
1st stage w/ masks	24.9	89.7	165.6	0.684

Table 1. **Ablation on training.** We show that our two-stage training strategy considerably boosts results and approaches an upper bound exploiting privileged information (1st stage w/ masks).

sons we compare only with the backbone CogVideoX in Figure 3, we include detailed comparisons against all baselines in the Appendix. We noticed that CogVideoX suffers from unrealistic interactions, making objects fly or disappear. Instead, KineMask generates realistic interactions with other objects if they are present in the path of motion of the initial moving object, showing a correct understanding of rigid body dynamics. We also show (Figure 3, bottom left) complex interactions that require implicit 3D understanding, making the glass of juice fall and crash as a result of motion, and multi-object motion and interactions (bottom right). Our realistic real world outputs show a strong generalization of the knowledge acquired from simulated videos.

User study. In Figure 4, we show results of a user study with 30 participants, who perform pairwise comparisons of videos generated by KineMask and baselines on *Real World*. Participants are presented with initial images and input object velocities indicated by arrows. We ask them to evaluate outputs on three different axes: motion fidelity to the control signal (Motion), realism of the object interactions (Interactions), overall physical consistency (Physical). Each answer is collected with a three-answer forced choice format, where we compare our outputs with baselines and we ask for user preferences, allowing also to reply “both have the same quality”. The full details are presented in Appendix A.2. The collected user preferences indicate that *our method significantly outperforms all baselines in all*

questions. This demonstrates that existing methods are unsuitable for rendering interactions with starting conditions only. Kinemask, instead, renders realistic interactions.

4.3. Analysis and ablation studies

4.3.1. Low-level motion control

In our first set of experiments, we evaluate KineMask on low-level motion control. To do so, we train KineMask on *Simple Motion* with a prompt $c_0 = \text{“An object moving on a surface”}$, hence discarding the rich description c extracted by Tarsier. At inference, we assume $c_{\text{infer}} = c_0$. Doing so, we isolate the effects of low-level conditioning from those of high-level textual control, allowing for a fair assessment of KineMask as a motion conditioning method.

Fine-grained control. In Figure 5, we present results on different degrees of freedom of KineMask. Despite being trained on basic synthetic data, KineMask generalizes motion control to complex real-world scenes, coherently with the findings in [20]. In particular, we show that KineMask achieves disentangled control over different directions, speed, and objects. This allows for a fine-grained evaluation of motion dynamics, precious for world modeling.

Two-stage training. In Table 1 we show the importance of our two-stage training introduced in Section 3.2. We test KineMask on *Simple Motion* only, to study the effects of motion control in isolation. We first report results of CogVideoX prompted with c as a lower bound. As additional baseline, we train directly ϕ'' (2nd stage only), without first-stage pretraining. As an upper bound, we also evaluate ϕ' using ground truth object masks provided for every frame at test time (1st stage w/ masks). Our two-stage strategy boosts considerably all metrics compared to training ϕ'' directly, approaching the upper bound. We noticed that the IoU is very sensitive to minor displacement errors of the moving objects (0.367 vs 0.684), that do not impact the overall quality of motion as captured by the other metrics.

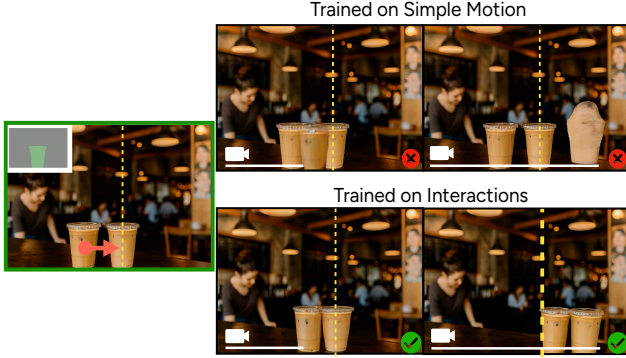


Figure 6. **Impact of training data.** While KineMask trained on *Simple Motion* is able to generalize to *Real World* images, the lack of object interactions in *Simple Motion* results in hallucinations (top). Training on *Interactions* results in collisions and plausible motion of pushed objects (bottom).

4.3.2. Impact of data

Next, we explore the effects of training data on KineMask for generating realistic rigid body interactions. We compare models trained on synthetic samples with and without interactions, and draw conclusions on the capability of VDMs to learn motion. We still use c_0 at both training and inference, as in Section 4.3.1.

Data influence. We evaluate KineMask’s capability to synthesize object interactions depending on the training data. We first test the model trained on *Simple Motion* and apply it to *Real World* data. We deliberately set input velocities to directions that should generate collisions among objects in the scene. The VDM fails to render realistic collisions (Figure 6, top). However, KineMask trained on the *Interactions* set produces accurate interactions for the same input velocities (Figure 6, bottom). Hence, *KineMask trained on appropriate data allows to render complex object interactions*. Moreover, this experiment yields important insights: while VDMs are robust to visual distribution shift, as even synthetic training data do not influence the realism of *Real World* generated scenes, their preservation of motion understanding seems to be more impacted, since training on *Simple Motion* prevents to generate interactions. This raises questions on VDMs catastrophic forgetting.

Quantitative evaluation. We validate the importance of specific data with a quantitative evaluation on *Interactions*, following the same protocol as in Section 4.3.1. As shown in Table 2, KineMask achieves the best results when trained on *Interactions*. Notably, even when trained only on *Simple Motion*, it greatly outperforms CogVideoX, highlighting the need of our research.

Method	Training	Interactions			
		MSE↓	FVD↓	FMVD↓	IoU↑
CogVideoX	-	344.6	807.3	3514.9	0.192
KineMask	<i>Simple Motion</i>	166.2	301.1	160.5	0.334
KineMask	<i>Interactions</i>	158.7	250.7	143.8	0.355

Table 2. **Effects of data.** Compared with models trained on *Simple Motion*, *Interactions* data considerably boosts performance.

Emergence of causality. Figure 7 shows results of KineMask trained on *Interactions* and tested with different inputs on a *Real World* scene with interacting objects. On top, as velocity increases, the interactions also change, indicating that the model captures causality of collisions. At the bottom, *with the same velocity*, we inpaint the input image, removing the interacting object, or replacing it with objects of different mass. The different final position of the moving object demonstrates understanding of mass in collisions. Note that this result is challenging for drag-based methods since they imply prior knowledge of the object final position. KineMask instead maps different target positions to the same input, depending on the environment.

4.3.3. High-level text conditioning

We now enable the usage of c at training and c_{infer} at inference. This allows us to assess the effects of text introduced in KineMask, and to draw insights on generalization.

Qualitative evaluation. We compare KineMask trained with c_0 against training with c , while using c_{infer} for inference in both cases. Doing so, we aim to evaluate the effects of textual prompts describing interactions during training. As shown in Figure 8, training with rich captions c allows the method to render interactions beyond those used for training, successfully exploiting the VDM prior knowledge in the rendered videos. Indeed, the model trained with c_0 fails to follow some effects in c_{infer} , such as vase breaking, or small waves forming. Instead, the model trained with c is able to benefit from additional information described in c_{infer} , correctly breaking the vase and perturbing the water. Please also note that the captions used in training are always tied to synthetic elements in *Interactions*, and therefore have limited diversity. Nevertheless, this still enables successful transfer to c_{infer} prompts describing complex effects that go beyond the training distribution of KineMask.

Quantitative evaluation. We also evaluate metrics with different textual conditioning in Table 3. We consider trainings with c_0 , using c_0 or c_{infer} at inference. Results demonstrate that using c at training time boosts object consistency (IoU 0.376 vs 0.356 of the second best configuration) and overall realism (FVD 231.3 vs 238.8, MSE on par), while we lose some motion consistency (FMVD

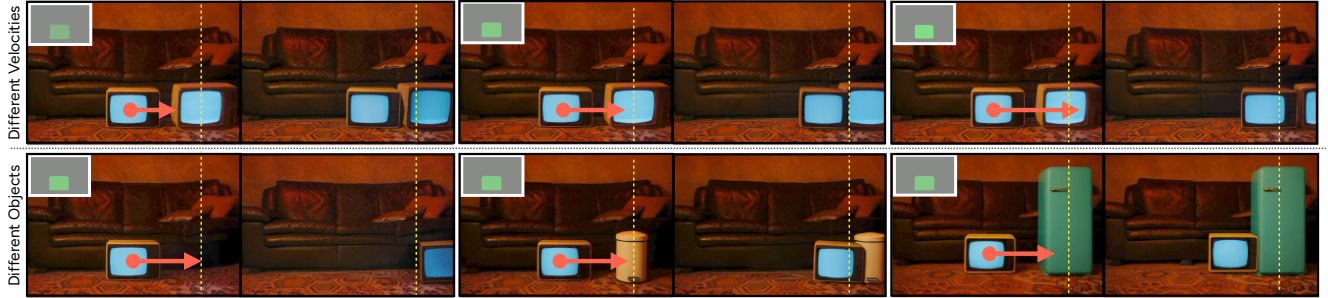


Figure 7. **Causality effects.** On top, we show how different velocity impacts motion effects, suggesting causal understanding. At the bottom, we show that the environment impacts rendering results for the same input velocity but different objects, suggesting mass awareness.

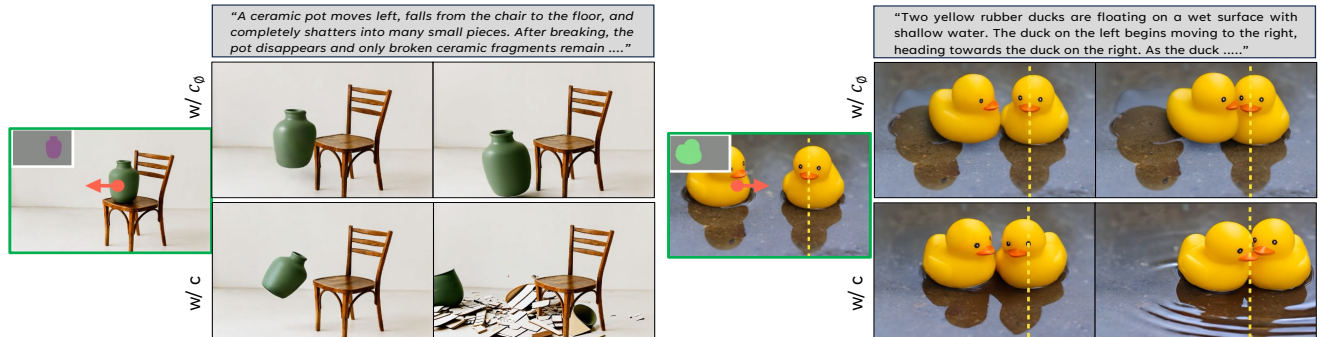


Figure 8. **Impact of text.** Training with rich captions c makes KineMask generate effects that go beyond the synthetic data used for training, exploiting the prior knowledge of the VDM. Indeed, while we prompt both models with c_{infer} , KineMask trained with c (bottom row) is able to generate complex effects of the interactions, such as crashing objects, and water effects. See the full prompts in Appendix A.2.

		<i>Interactions</i>			
Train	Infer	MSE ↓	FVD ↓	FMVD ↓	IoU ↑
c_{\emptyset}	c_{\emptyset}	158.7	250.7	143.8	0.355
c_{\emptyset}	c_{infer}	174.4	238.8	161.3	0.356
c	c_{infer}	160.9	231.3	174.4	0.376

Table 3. **Ablation on captions.** Training with c , we improve object consistency and general quality on synthetic data.

174.4 vs 143.8 of the best model). However, note that Table 3 includes *only evaluation on synthetic data*, where we have access to a motion ground truth. Considering the improved qualitatives on *Real World* and the benefit on complex interactions (see Figure 8) we believe the use of captions c during training is still beneficial for the final model to improve robustness and preserve its capabilities.

5. Discussion

We introduced KineMask, a framework to enable video generation of object interactions and effects in complex scenes. Our experiments show that KineMask achieves significant improvements over state-of-the-art models of com-

parable size, synthesizing realistic multi-object interactions while allowing control over variable object velocities. We believe this methodology can inform future work on world models, with potential implications for robotic manipulation, planning, and embodied decision making.

Limitations and future work. While effective, KineMask’s low-level conditioning is limited to velocity, whereas real-world motion also depends on factors such as friction, shape, mass, and air resistance. Incorporating such controls is a promising direction for making VDM-generated motion more physically accurate. Moreover, we believe that extending to soft-body interactions will further improve world modeling capabilities. In our inference pipeline on real images (Section 3.3), we further use ChatGPT to generate textual descriptions of rigid-body interactions. As shown in Section 4.3.3, combining text-based conditioning with KineMask enhances realism, highlighting the complementary roles of high-level textual guidance and low-level video control. These results support the joint use of both modalities for physically grounded world modeling, and we speculate that advances in multimodal language models [51, 52] may enable text-based physical reasoning to complement video generation.

References

- [1] Hassan Abu Alhaja, Jose Alvarez, Maciej Bala, et al. Cosmos-transfer: Conditional world generation with adaptive multimodal control. *arXiv*, 2025. 2
- [2] Niket Agarwal, Arslan Ali, Maciej Bala, Yogesh Balaji, Erik Barker, Tiffany Cai, Prithvijit Chattopadhyay, Yongxin Chen, Yin Cui, Yifan Ding, et al. Video diffusion models. In *NeurIPS*, 2022. 2
- [3] Niket Agarwal, Arslan Ali, Maciej Bala, Yogesh Balaji, Erik Barker, Tiffany Cai, Prithvijit Chattopadhyay, Yongxin Chen, Yin Cui, Yifan Ding, et al. Cosmos world foundation model platform for physical ai. *arXiv*, 2025. 1, 2
- [4] Rick Akkerman, Haiwen Feng, Michael J Black, Dimitrios Tzionas, and Victoria Fernández Abrevaya. Interdyn: Controllable interactive dynamics with video diffusion models. In *CVPR*, 2025. 3, 4
- [5] Eloi Alonso, Adam Jelley, Vincent Micheli, Anssi Kanervisto, Amos J Storkey, Tim Pearce, and François Fleuret. Diffusion for world modeling: Visual details matter in atari. *NeurIPS*, 2024. 1, 2
- [6] AmbientCG. AmbientCG. [Link](#), 2018-2025. 4
- [7] Omer Bar-Tal, Hila Chefer, Omer Tov, Charles Herrmann, Roni Paiss, et al. Lumiere: A space-time diffusion model for video generation. In *SIGGRAPH Asia*, 2024. 2
- [8] Andreas Blattmann, Timo Milbich, Michael Dorkenwald, and Björn Ommer. ipoke: Poking a still image for controlled stochastic video synthesis. In *ICCV*, 2021. 2
- [9] Andreas Blattmann, Tim Dockhorn, Sumith Kulal, Shuyang Tang, Zhendong Wang, Patrick Esser, and Robin Rombach. Stable video diffusion: Scaling latent video diffusion models to large datasets. *arXiv preprint arXiv:2311.15127*, 2023. 2
- [10] Andreas Blattmann, Robin Rombach, Huan Ling, Tim Dockhorn, Seung Wook Kim, Sanja Fidler, and Karsten Kreis. Align your latents: High-resolution video synthesis with latent diffusion models. In *CVPR*, 2023. 1
- [11] Ryan Burgert, Yuancheng Xu, Wenqi Xian, Oliver Pilarski, Pascal Clausen, Mingming He, Li Ma, Yitong Deng, Lingxiao Li, Mohsen Mousavi, et al. Go-with-the-flow: Motion-controllable video diffusion models using real-time warped noise. In *CVPR*, 2025. 2
- [12] Kyle Chayka. An a.i.-generated film depicts human loneliness, in ‘thank you for not answering’. [Link](#), 2023. 1
- [13] Boyuan Chen, Hanxiao Jiang, Shaowei Liu, Saurabh Gupta, Yunzhu Li, Hao Zhao, and Shenlong Wang. Physgen3d: Crafting a miniature interactive world from a single image. In *CVPR*, 2025. 1, 2, 16
- [14] Haoxin Chen, Menghan Xia, Yingqing He, Yong Zhang, Xiaodong Cun, Xintao Wang, Ying Shan, and Xiu Li. Videocrafter: Open diffusion models for high-quality video generation. *arXiv*, 2023. 2
- [15] Tsai-Shien Chen, Chieh Hubert Lin, Hung-Yu Tseng, Tsung-Yi Lin, and Ming-Hsuan Yang. Motion-conditioned diffusion model for controllable video synthesis. *arXiv preprint arXiv:2304.14404*, 2023. 1
- [16] Aram Davtyan and Paolo Favaro. Learn the force we can: Enabling sparse motion control in multi-object video generation. In *AAAI*, 2024. 2
- [17] Yufan Deng, Ruida Wang, Yuhao Zhang, Yu-Wing Tai, and Chi-Keung Tang. Dragvideo: Interactive drag-style video editing. In *ECCV*. Springer, 2024. 2
- [18] Zihan Ding, Amy Zhang, Yuandong Tian, and Qingqing Zheng. Diffusion world model: Future modeling beyond step-by-step rollout for offline reinforcement learning. *arXiv*, 2024. 1
- [19] Daniel Geng, Charles Herrmann, Junhwa Hur, Forrester Cole, Serena Zhang, Tobias Pfaff, Tatiana Lopez-Guevara, Carl Doersch, Yusuf Aytar, Michael Rubinstein, Chen Sun, Oliver Wang, Andrew Owens, and Deqing Sun. Motion prompting: Controlling video generation with motion trajectories. In *CVPR*, 2025. 1, 2
- [20] Nate Gillman, Charles Herrmann, Michael Freeman, Daksh Aggarwal, Evan Luo, Deqing Sun, and Chen Sun. Force prompting: Video generation models can learn and generalize physics-based control signals. In *NeurIPS*, 2025. 1, 3, 5, 6
- [21] Yuwei Guo, Ceyuan Yang, Anyi Rao, Maneesh Agrawala, Dahua Lin, and Bo Dai. Sparsectrl: Adding sparse controls to text-to-video diffusion models. In *ECCV*, 2024. 2
- [22] Yuwei Guo, Ceyuan Yang, Anyi Rao, Zhengyang Liang, Yaohui Wang, Yu Qiao, Maneesh Agrawala, Dahua Lin, and Bo Dai. Animatediff: Animate your personalized text-to-image diffusion models without specific tuning. *ICLR*, 2024. 2
- [23] David Ha and Jürgen Schmidhuber. World models. In *NeurIPS*, 2018. 1
- [24] Yoav HaCohen, Nisan Chiprut, Benny Brazowski, Daniel Shalem, Dudu Moshe, et al. Ltx-video: Realtime video latent diffusion. *arXiv*, 2024. 2
- [25] Jonathan Ho, Ajay Jain, and Pieter Abbeel. Denoising diffusion probabilistic models. *NeurIPS*, 2020. 1
- [26] Anthony Hu, Lloyd Russell, Hudson Yeo, Zak Murez, George Fedoseev, Alex Kendall, Jamie Shotton, and Gianluca Corrado. Gaia-1: A generative world model for autonomous driving. *arXiv*, 2023. 2
- [27] Zhihao Hu and Dong Xu. Videocontrolnet: Motion-guided video-to-video translation via diffusion models. In *ICLR*, 2024. 2
- [28] Tianyu Huang, Haoze Zhang, Yihan Zeng, Zhilu Zhang, Hui Li, Wangmeng Zuo, and Rynson WH Lau. Dreamphysics: Learning physics-based 3d dynamics with video diffusion priors. In *AAAI*, 2025. 2
- [29] Aaron Hurst, Adam Lerer, Adam P Goucher, Adam Perelman, Aditya Ramesh, Aidan Clark, AJ Ostrow, Akila Welihinda, Alan Hayes, Alec Radford, et al. Gpt-4o system card. *arXiv*, 2024. 5
- [30] Bingyi Kang, Yang Yue, Rui Lu, Zhijie Lin, Yang Zhao, Kaixin Wang, Gao Huang, and Jiashi Feng. How far is video generation from world model: A physical law perspective. In *ICML*, 2025. 1
- [31] Wenbo Kong, Wenbo Dong, Dong Wang, Yang Li, et al. Hunyuanvideo: A systematic framework for large video generative models. *arXiv*, 2024. 1, 2
- [32] Guojun Lei, Chi Wang, Rong Zhang, Yikai Wang, Hong Li, and Weiwei Xu. Animateanything: Consistent and control-

- lable animation for video generation. In *CVPR*, 2025. 1, 2
- [33] Chenyu Li, Oscar Michel, Xichen Pan, Sainan Liu, Mike Roberts, and Saining Xie. Pisa experiments: Exploring physics post-training for video diffusion models by watching stuff drop. In *ICML*, 2025. 3
- [34] Haonan Li, Xueyan Zhang, Wei Xu, Jing Liu, and Yizhou Wang. Keyvid: Video generation with keyframe propagation and temporal control. *arXiv:2403.12006*, 2024. 2
- [35] Xiang Li, Dahua Lin, and Bo Dai. Motionctrl: A unified model for controllable text-to-motion generation. In *SIGGRAPH*, 2024. 1, 2
- [36] Yuhao Li, Mirana Claire Angel, Salman Khan, Yu Zhu, Jinqiu Sun, Yanning Zhang, and Fahad Shahbaz Khan. C-drag: Chain-of-thought driven motion controller for video generation. *arXiv*, 2025. 2
- [37] Zizhang Li, Hong-Xing Yu, Wei Liu, Yin Yang, Charles Herrmann, Gordon Wetzstein, and Jiajun Wu. Wonderplay: Dynamic 3d scene generation from a single image and actions. In *ICCV*, 2025. 1, 2
- [38] Jiahe Liu, Youran Qu, Qi Yan, Xiaohui Zeng, Lele Wang, and Renjie Liao. Frechet video motion distance: A metric for evaluating motion consistency in videos. In *ICML*, 2024. 5
- [39] Shaowei Liu, Zhongzheng Ren, Saurabh Gupta, and Shenglong Wang. Physgen: Rigid-body physics-grounded image-to-video generation. In *ECCV*, 2024. 1, 2
- [40] Harri Miller. Elvis is back in the building, thanks to ai—and u2. *Link*, 2023. 1
- [41] Saman Motamed, Laura Culp, Kevin Swersky, Priyank Jaini, and Robert Geirhos. Do generative video models understand physical principles? *arXiv*, 2025. 1
- [42] Chong Mou, Yingqing Zhou, Xintao Song, Yibing Ge, Wei Liu, Yufei Zhang, Qifeng Wang, and Ying Shan. T2i-adapter: Learning adapters to dig out more controllable ability for text-to-image diffusion models. In *AAAI*, 2024. 2
- [43] OpenAI. GPT-5 System Card. *Link*, 2025. 4
- [44] William Peebles and Saining Xie. Scalable diffusion models with transformers. In *ICCV*, 2023. 2
- [45] Alexander Pondaven, Aliaksandr Siarohin, Sergey Tulyakov, Philip Torr, and Fabio Pizzati. Video motion transfer with diffusion transformers. In *CVPR*, 2025. 2
- [46] Nikhila Ravi, Valentin Gabeur, Yuan-Ting Hu, Ronghang Hu, Chaitanya Ryali, Tengyu Ma, Haitham Khedr, Roman Rädle, Chloe Rolland, Laura Gustafson, et al. Sam 2: Segment anything in images and videos. In *ICLR*, 2025. 4, 5
- [47] Emma Roth. Kalshi’s surreal \$2,000 ai-generated ad aired during the nba finals. *Link*, 2025. 1
- [48] Lloyd Russell, Anthony Hu, Lorenzo Bertoni, George Fedoseev, Jamie Shotton, Elahe Arani, and Gianluca Corrado. Gaia-2: A controllable multi-view generative world model for autonomous driving. *arXiv*, 2025. 2
- [49] Xiaoyu Shi, Zhaoyang Huang, Fu-Yun Wang, Weikang Bian, Dasong Li, Yi Zhang, Manyuan Zhang, Ka Chun Cheung, Simon See, Hongwei Qin, et al. Motion-i2v: Consistent and controllable image-to-video generation with explicit motion modeling. In *SIGGRAPH 2024*, 2024. 2, 5
- [50] Yongqing Shi, Shaoteng Liu, Hang Zhou, Rui Yang, and Yu Qiao. Dragdiffusion: Harnessing diffusion models for interactive point-based image editing. In *CVPR*, 2024. 1, 2
- [51] Mustafa Shukor, Enrico Fini, Victor Guilherme Turrissi da Costa, Matthieu Cord, Joshua Susskind, and Alaaeldin El-Nouby. Scaling laws for native multimodal models. In *ICCV*, 2025. 8
- [52] Gemini Team, Rohan Anil, Sebastian Borgeaud, Jean-Baptiste Alayrac, Jiahui Yu, Radu Soricut, Johan Schalkwyk, Andrew M Dai, Anja Hauth, Katie Millican, et al. Gemini: a family of highly capable multimodal models. *arXiv*, 2023. 8
- [53] Thomas Unterthiner, Sjoerd Van Steenkiste, Karol Kurach, Raphaël Marinier, Marcin Michalski, and Sylvain Gelly. Fvd: A new metric for video generation. In *ICLR Workshops*, 2019. 5
- [54] Dani Valevski, Yaniv Leviathan, Moab Arar, and Shlomi Fruchter. Diffusion models are real-time game engines. In *ICLR*, 2025. 2
- [55] Team Wan, Ang Wang, Baole Ai, Bin Wen, Chaojie Mao, Chen-Wei Xie, Di Chen, Feiwu Yu, Haiming Zhao, Jianxiao Yang, et al. Wan: Open and advanced large-scale video generative models. *arXiv*, 2025. 2, 5
- [56] Zhang Wan, Sheng Tang, Jiawei Wei, Ruize Zhang, and Juan Cao. Dragentity: Trajectory guided video generation using entity and positional relationships, 2024. 2
- [57] Jiuniu Wang, Hangjie Yuan, Dayou Chen, Yingya Zhang, Xiang Wang, and Shiwei Zhang. Modelscape text-to-video technical report. *arXiv*, 2023. 2
- [58] Jiawei Wang, Liping Yuan, Yuchen Zhang, and Haomiao Sun. Tarsier: Recipes for training and evaluating large video description models. In *ICLR*, 2025. 5, 12
- [59] Yaohui Wang, Xinyuan Chen, Xin Ma, Shangchen Zhou, Ziqi Huang, Yi Wang, Ceyuan Yang, Yinan He, Jiashuo Yu, Peiqing Yang, Yuwei Guo, Tianxing Wu, Chenyang Si, Yuming Jiang, Cunjian Chen, Chen Change Loy, Bo Dai, Dahua Lin, Yu Qiao, and Ziwei Liu. Lavie: High-quality video generation with cascaded latent diffusion models. *International Journal of Computer Vision*, 133(5):3059–3078, 2025. 2
- [60] Thaddäus Wiedemer, Yuxuan Li, Paul Vicol, Shixiang Shane Gu, Nick Matarese, Kevin Swersky, Been Kim, Priyank Jaini, and Robert Geirhos. Video models are zero-shot learners and reasoners. *arXiv preprint arXiv:2509.20328*, 2025. 1
- [61] Zhuoyi Yang, Jiayan Teng, Wendi Zheng, Ming Ding, Shiyu Huang, et al. Cogvideox: Text-to-video diffusion models with an expert transformer. In *ICLR*, 2025. 1, 2, 5
- [62] Shengming Yin, Chenfei Wu, Jian Liang, Jie Shi, Houqiang Li, Gong Ming, and Nan Duan. Dragnuwa: Fine-grained control in video generation by integrating text, image, and trajectory. *arXiv preprint arXiv:2308.08089*, 2023. 2
- [63] Lvmin Zhang, Anyi Rao, and Maneesh Agrawala. Adding conditional control to text-to-image diffusion models. In *ICCV*, 2023. 2, 3
- [64] Tianyuan Zhang, Hong-Xing Yu, Rundi Wu, Brandon Y Feng, Changxi Zheng, Noah Snively, Jiajun Wu, and William T Freeman. Physdreamer: Physics-based interaction with 3d objects via video generation. In *European Con-*

ference on Computer Vision, pages 388–406. Springer, 2024. [2](#)

- [65] Yuang Zhang, Jiayi Gu, Li-Wen Wang, Han Wang, Junqi Cheng, Wen Zheng, and Changjie Fan. Mimicmotion: High-quality human motion video generation with confidence-aware pose guidance. In *CVPR*, 2024. [2](#)
- [66] Zhenghao Zhang, Junchao Liao, Menghao Li, Zuoqun Dai, Bingxue Qiu, Siyu Zhu, Long Qin, and Weizhi Wang. Tora: Trajectory-oriented diffusion transformer for video generation. In *CVPR*, 2025. [1](#), [2](#), [5](#)
- [67] Shihao Zhao, Dongdong Chen, Yen-Chun Chen, Jianmin Bao, Lu Yuan, Dongdong Wang, and Kwan-Yee K. Wong. Uni-controlnet: All-in-one control to text-to-image diffusion models. In *NeurIPS*, 2023. [2](#)
- [68] Haitao Zhou, Chuang Wang, Rui Nie, Jinlin Liu, Dongdong Yu, Qian Yu, and Changhu Wang. Trackgo: A flexible and efficient method for controllable video generation. In *AAAI*, 2025. [1](#), [2](#)

A. Appendix

A.1. Video qualitative results

For a comprehensive qualitative evaluation on videos, we refer the reader to the attached supplementary material, in which we provide qualitative examples for all *Real World* images animated with KineMask and baselines. We organize the results by using a website that can be easily opened in any browser. To visualize the videos, simply click on the `KineMask-main/index.html` file after unzipping the material. Please note that for transparency we include randomly selected outputs from all images in *Real World* and common failure cases.

A.2. Additional details

Used prompts We report here the prompt used for c generation at training time and c_{infer} used for inference time. We prompt Tarsier [58] to extract c with: *“Describe the video in a concise way, covering all motions and collisions between objects.”*. This simple prompt is already resulting in sufficiently good descriptions. For inference, instead, we rely on GPT prompting with in-context learning examples to extract suitable descriptions. We report the prompt below, along the associated in-context examples in Figure 11.

Inference-time c_{infer} generation prompt

Reference: The first five attached examples are the first frames of simulated videos that contain multiple objects on a surface, in each example one or two objects can start moving, and these objects can or cannot collide with other objects depending on their initial velocity and direction. The range of velocities for the initial motion of these objects is from 0.5m/s to 1.5m/s.

- In the first initial frame the green cube moves at 1.23m/s and the red cylinder at 1.07m/s. The entire video description for this video is: “On a wooden floor, there are four objects: a red cylinder, a green cube, a yellow cube, and a white cylinder. The red cylinder starts in the center and moves to the right, while the green cube moves to the left. The red cylinder continues to move to the right and eventually collides slightly with the white cylinder. The green cube continues to move left and collides slightly with the yellow cube. The red cylinder and the white cylinder remain stationary after the collision.”.

- In the second initial frame the white cube moves at 0.67m/s and the purple cube at 1.35m/s, the entire description for this video is: “On a grassy background, there are a yellow cylinder, a purple cube, a pink cube, and a white cube. The white cube moves towards the yellow cylinder and collides slightly with it. The white cube then stops next to the yellow cylinder. The purple cube moves towards the pink cube and collides with it, moving it towards the top right, after the collision all objects remain stationary.”.

- In the third initial frame the white cube moves at 1.5m/s and the light blue cube at 1.43m/s, the entire description for this video is: “Four cubes of different colors (yellow, green, blue, and purple) are on a textured, brown surface. The blue cube moves towards the green cube, colliding with it and pushing it downwards. The yellow cube moves towards the pink cube, they collide and the purple cube moves out of the frame. After the collision the blue and green cylinder are static next to each other, while the yellow cube is positioned in the top right part of the frame.”.

- In the fourth initial frame, the gray cube moves at 0.64m/s, the entire description for this video is: “The scene is set on a brick ground with patches of green moss. A white cylinder is stationary in the background. A gray cube, initially positioned on the left side of the frame, moves

horizontally to the right and eventually stops in the center of the frame. Two pink cubes, one on the right side and another slightly behind it, remain stationary throughout the sequence.”.

- In the fifth initial frame the white cylinder moves at 0.71m/s and the pink cylinder moves at 0.55m/s. The entire description for this video is: “The scene consists of a grassy background with four 3D shapes: a purple cube, a white cylinder, a pink cylinder, and another purple cube. The white cylinder and the pink cylinder move slightly to the left. The purple cubes in the foreground remain stationary throughout the sequence.”.

Objective: -The last attached initial frame consists of a real picture, in this case the xxx on the xxx moves to the xxx at xxxm/s !!. According to this information and taking into account the provided examples from simulated videos, please provide an entire description, predicting what is going to happen in this scene. The provided video description should follow the same style and words used in the given simulated examples !!, reason about the real scene and describe if collisions happen or not, if they do, describe them, consider the distance and velocity between objects in the real scene to determine how the objects move, and how strong the collisions are. Make sure the description would include realistic effects if they happen produced by the movement or collisions that may occur between objects, for example movement of liquids, steam effects, falling objects, etc. If these effects are not present in the scene please do not include anything related to them in the prompt !!. Do not include velocity values in it, friction effects, information from the surface, inclinations, rotations, or produced sounds.

Training Hyperparameters We train KineMask using bf16 mixed precision for 1000 steps with a total batch size of 40 and saved checkpoints every 250 steps. Our backbone is initialized from the pretrained THUDM/CogVideoX-5b-I2V model. For the Controlnet we used the first 8 transformer layers, a downscaling factor of 8 and a control-weight of 0.5. We use AdamW optimizer with a learning rate of 1×10^{-4} , $\beta_1=0.9$, $\beta_2=0.95$, a cosine-with-restart learning-rate schedule and a max gradient norm of 1.0.

Baseline implementation details We compare KineMask with Force Prompting, TORA, Motion-I2V, CogvideoX and Wan. All methods use an input prompt and an initial image. Additionally, Force Prompting takes the point coordinates of where to apply the force, the force prompt, and the angle of movement. Tora and Motion-I2V need the entire motion trajectory, we give the initial and final points. In all cases, we apply the same prompt c_{infer} that we extract by querying GPT. In the extracted prompts, the moving object and its interactions are always described.

Synthetic Samples Figure 9 shows our synthetic dataset along with the velocity masks for each case. Please note that the masks are extracted only for objects that move at the beginning of the video, these change their color and intensity depending on motion direction and velocity magnitude.

Prompts for Figure 8 We report here the prompts for rendering Figure 8, that we omitted due to the lack of space.

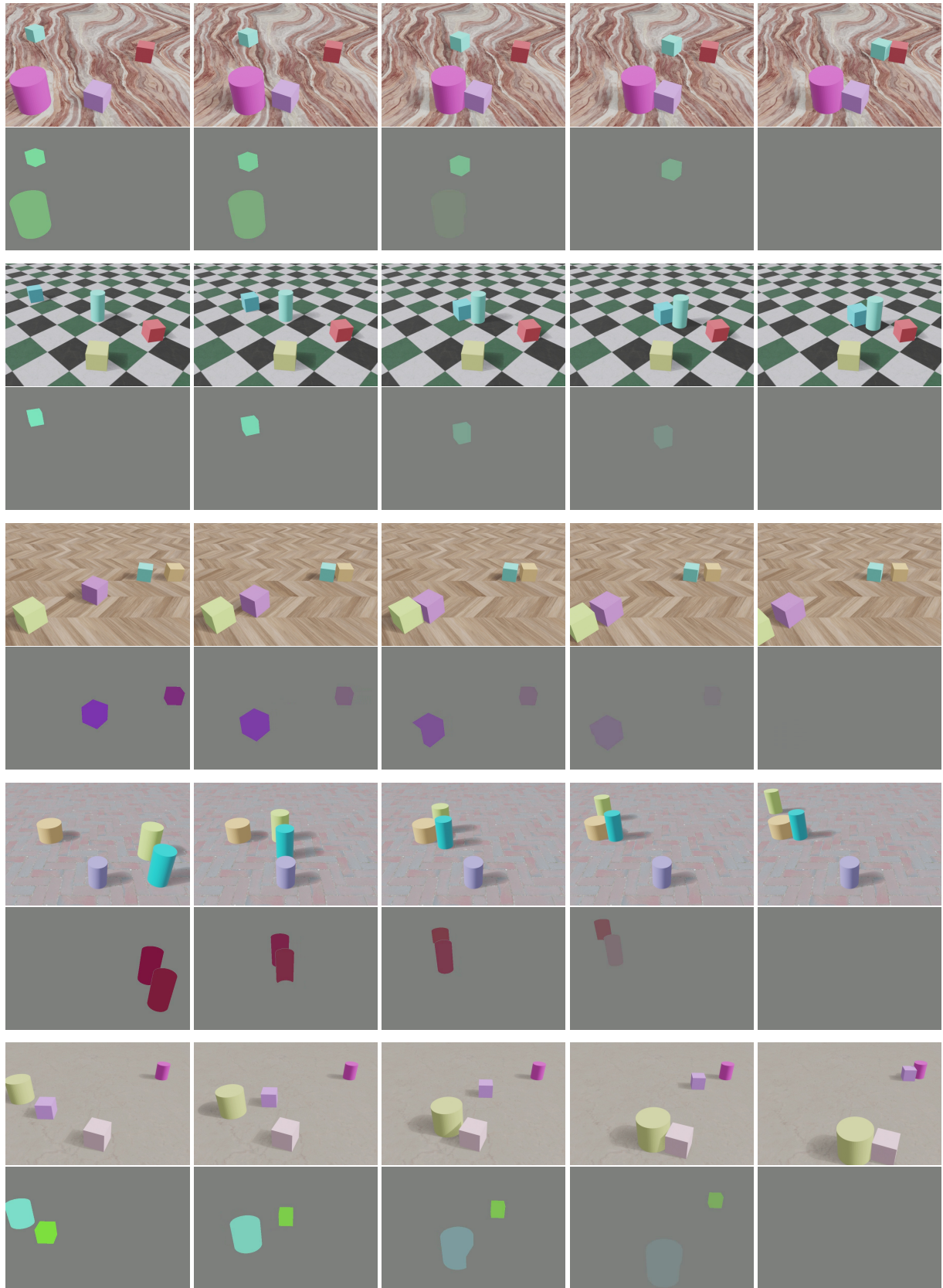


Figure 9. Samples from our synthetic videos and velocity masks used as training dataset.



Figure 10. Qualitative comparison with all baselines.



Figure 11. **In-context learning examples.** Providing examples to GPT helps the generation of the text c_{infer} following a desired format.

Full Prompt Figure 8 (left)

"A ceramic pot moves left, falls from the chair to the floor, and completely shatters into many small pieces. After breaking, the pot disappears and only broken ceramic fragments remain scattered on the floor."

Full Prompt Figure 8 (right)

"Two yellow rubber ducks are floating on a wet surface with shallow water. The duck on the left begins moving to the right, heading towards the duck on the right. As the duck on the left advances, small ripples spread outward from its base, disturbing the water. The duck on the left continues its motion and collides firmly with the duck on the right. The impact creates overlapping ripples and small splashes around both ducks. The duck on the right shifts to the side, while the duck on the left comes to a stop next to it. After the collision, the water ripples gradually spread and fade, and both ducks remain stationary."

Details for user study We now provide additional details for our user study. First, we divide users into 5 groups, randomizing the videos to display to limit the time necessary to complete our study. We display the videos in couples, along the original frame with the represented control, via a Telegram bot specifically used for the task and represented in Figure 14. For each video pair, we ask:

1. Which of these two outputs follow better the motion indicated by the arrow in terms of direction?
2. Which of the two outputs has the most realistic object interactions?
3. Which of the two outputs have the best overall physical realism?

We aggregate replies from all users in order to build the plots in Figure 4.

A.3. Additional results

Test on different model backbones We tested our proposed approach on two model backbones CogVideoX-5B-I2V and Wan2.2-I2V-5B, and performed a quantitative comparison on the evaluation set of our generated synthetic data, by training and testing on *Interactions*. Table 4 shows that both KineMasks versions outperform their original zero-shot backbones by large margins respectively. On the other hand, we noticed that KineMask-CogVideoX achieves better performances than its Wan counterpart, which also relates when comparing the performance of the original backbones when these are tested in a zero-shot manner, where CogVideoX achieves better performances than Wan. Fig-

		<i>Interactions</i>			
Backbone	Setup	MSE↓	FVD↓	FMVD↓	IoU↑
Wan	Baseline	431.4	977.7	3649.8	0.192
	KineMask	211.0	475.6	968.4	0.257
CogVideoX	Baseline	344.6	807.3	3514.9	0.192
	KineMask	158.7	250.7	143.8	0.355

Table 4. **Comparison of different model backbones.** We compare two versions of KineMask using different base models.

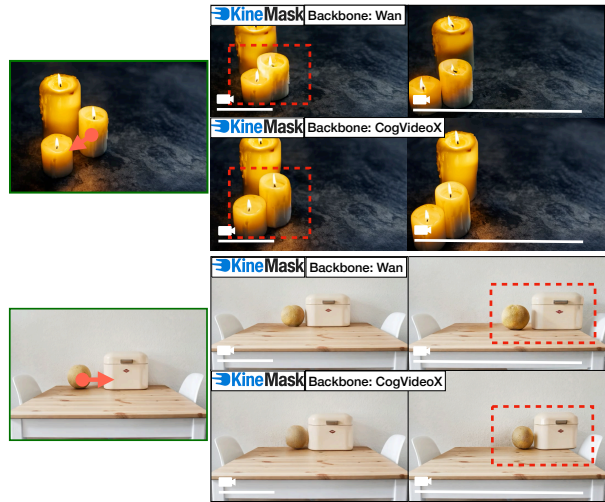


Figure 12. Comparison of model backbones.

ure 12 shows a comparison of real-world generations using KineMasks with both backbones. We noticed that while both backbones generate plausible object interactions, the model that used CogVideoX as backbone showed better object consistency. For example, using KineMask-Wan in Figure 12 top, the candles show some overlapping (Red Square) when the collision is generated, similarly in Figure 12 bottom, the fruit increased its size after the collision. On the other hand, we noticed that using KineMask-CogVideoX we obtained better rigid-body collisions. Due to this, we chose KineMask-CogVideoX (KineMask) as our main model.

Qualitative comparison against all baselines Figure 10 presents a complete qualitative comparison between Kine-

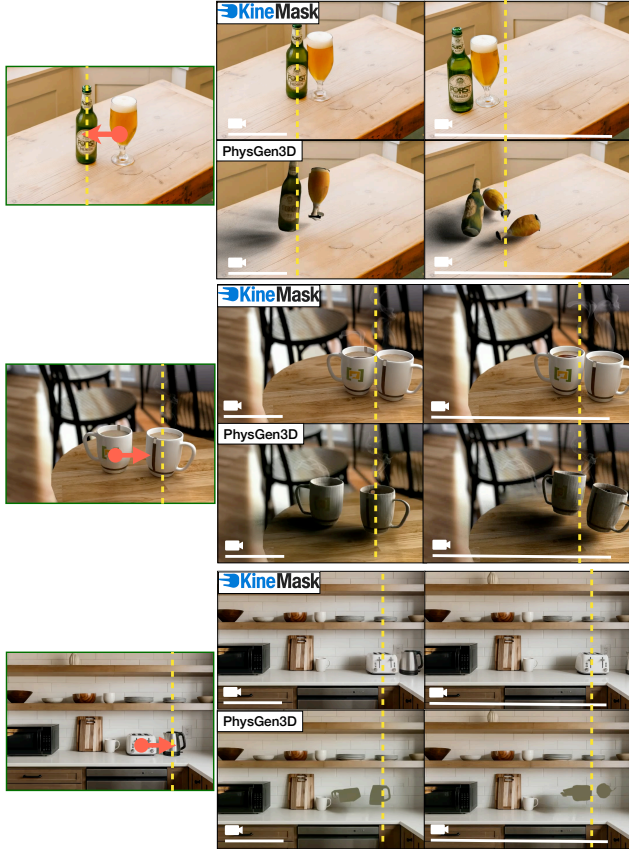


Figure 13. Qualitative comparison of KineMask vs PhysGen3D.

Mask and all baselines. Beyond the issues observed with CogVideoX (discussed in Section 4.2), Wan exhibits strong hallucinations and unrealistic object interactions. On the other hand, Drag-based methods such as Force-Prompting and Motion-I2V commonly suffer from slow object motion when objects are moved toward others, failing to synthesize proper interactions. Finally, TORA often produces hallucinations and ignores collisions, resulting in objects being placed incorrectly or stacked on top of one another. KineMask successfully generate plausible motion and object collisions according to the user input, showing its capability to correctly understand causality, and dynamics created due to collisions, and showing the generalization of the knowledge obtained from synthetic data in complex real-world scenes, even when some 3D understanding is necessary in order to render collisions with the floor.

Additional Qualitative Comparison In addition to comparing with our initial set of baselines, we also perform an additional qualitative comparison with the recent PhysGen3D [13], which uses 3D information, a simulator in the loop and a diffusion model as a rendering tool to generate plausible videos from an initial image. While this

<i>Interactions</i>				
Encoding	MSE↓	FVD↓	FMVD↓	IoU↑
v_0	205.7	277.3	216.3	0.294
v_t (ours)	160.9	231.3	174.4	0.376

(a) Velocity encoding

<i>Interactions</i>				
Sampling	MSE↓	FVD↓	FMVD↓	IoU↑
Uniform	232.0	303.1	190.9	0.323
Non-uniform (ours)	160.9	231.3	174.4	0.376

(b) Non-uniform sampling

Table 5. **Additional ablation studies.** We report an additional encoding strategies for our conditioning masks in Table ((a)), proving that our design choice of using v_t is best. Furthermore, we showcase that removing our non-uniform sampling on interactions-rich frames during dropout harms performance ((b)).

brings plausible physics due to the dynamics simulator, this causes multiple problems and limitations, from the complexity of the pipeline, dependency on the 3D reconstruction, and the lack of visual realism. As shown in Figure 13, PhysGen3D is vulnerable and dependent on its 3D reconstruction setup, which can cause incorrect object reconstructions, such as creating duplicated objects, like in the first case where the beer is created twice, or in the third example where the reconstruction is incorrect, causing a chain of failures towards synthesizing proper rigid-body interactions. Beyond the synthetic appearance to objects, PhysGen3D and simulation-based methods also are unable to generate effects like liquid or steam moving as a result of a collision, as shown in the second example where two cups collide. On the other hand, KineMask synthesizes plausible object collisions and effects created from object interactions, showing its understanding of rigid-body dynamics.

Velocity encoding We propose an ablation on our encoding mechanism. In KineMask, we assume to encode the instantaneous velocity of objects in frame t , hence v_t . This leads to barely visible masks in the presence of low velocity magnitude when the velocity decreases in presence of interactions. We have tested another configuration, by encoding instead for each frame the initial velocity v_0 , thus having well-defined masks for all the motion trajectory. However, from the results in Table 5a, we see that encoding the per frame velocity v_t yields better results. We speculate that this strategy would help the model understand the decrease trend of velocity that naturally occurs in motion, ultimately serving as an implicit regularization term for training.

Dropout density Section 4.1 mentioned that we sample non-uniformly the frame f^* for our second-stage training.

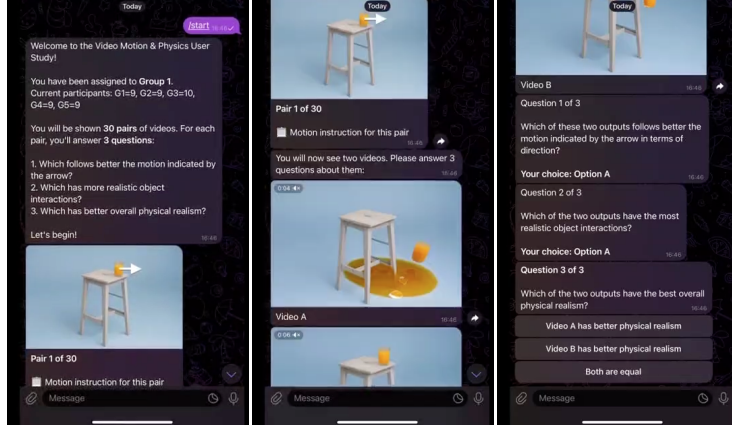


Figure 14. **User study interface.** We collect pairwise user preference on direction, interactions realism, and consistency of objects.

In Table 5b, we present a quantitative evaluation of the effects of this design. As visible, sampling the dropout around the frames where collisions occur in the training set helps KineMask to focus on interaction-rich representations.

Handling complex objects In Figure 15, we report an interesting failure mode of drag-based baselines successfully handled by KineMask. As visible, Force Prompting, TORA and Motion-I2V struggle when the control is applied to object with thin support structures, or with piled objects. This is the result of an architectural decision, since their control mechanism does not employ masks for identifying the object to move with pixel level precision. Instead, KineMask correctly generates motion on these edge cases. This shows how the presence of a dense mask brings a lot of benefits to perform better motion control in ambiguous cases compared to sparse conditioning information.

Failure Cases Figure 17 shows some failure cases of KineMask. In the first and second case, we have found that objects that do not have a considerable height tend to ignore others during their motion, thus a collision is not created. The third and fourth cases, show complex scenarios with many objects. This sometimes creates ambiguities, by resulting in object duplication or disappearance. We speculate here that the text prompt may also encourage ambiguity, due to the presence of multiple elements that can be associated to the same textual identifier.

Qualitatives For ease of visualization, we report in Figure 16 some additional qualitative results of interactions rendered with KineMask. As visible, in several real scenarios, we are able to render realistic object interactions, where objects move coherently with the users’ prompt.

A.4. LLM usage

In this research, we used GPT-5, to aid writing. The usage was limited to polishing some sentences and grammatical

checks, as well as to identifying inconsistencies in the used terminologies.



Figure 15. **Motion control comparison.** Our mask-based control is robust to ambiguous scenes, while other methods suffer from hallucinations due to the ambiguous control signal.

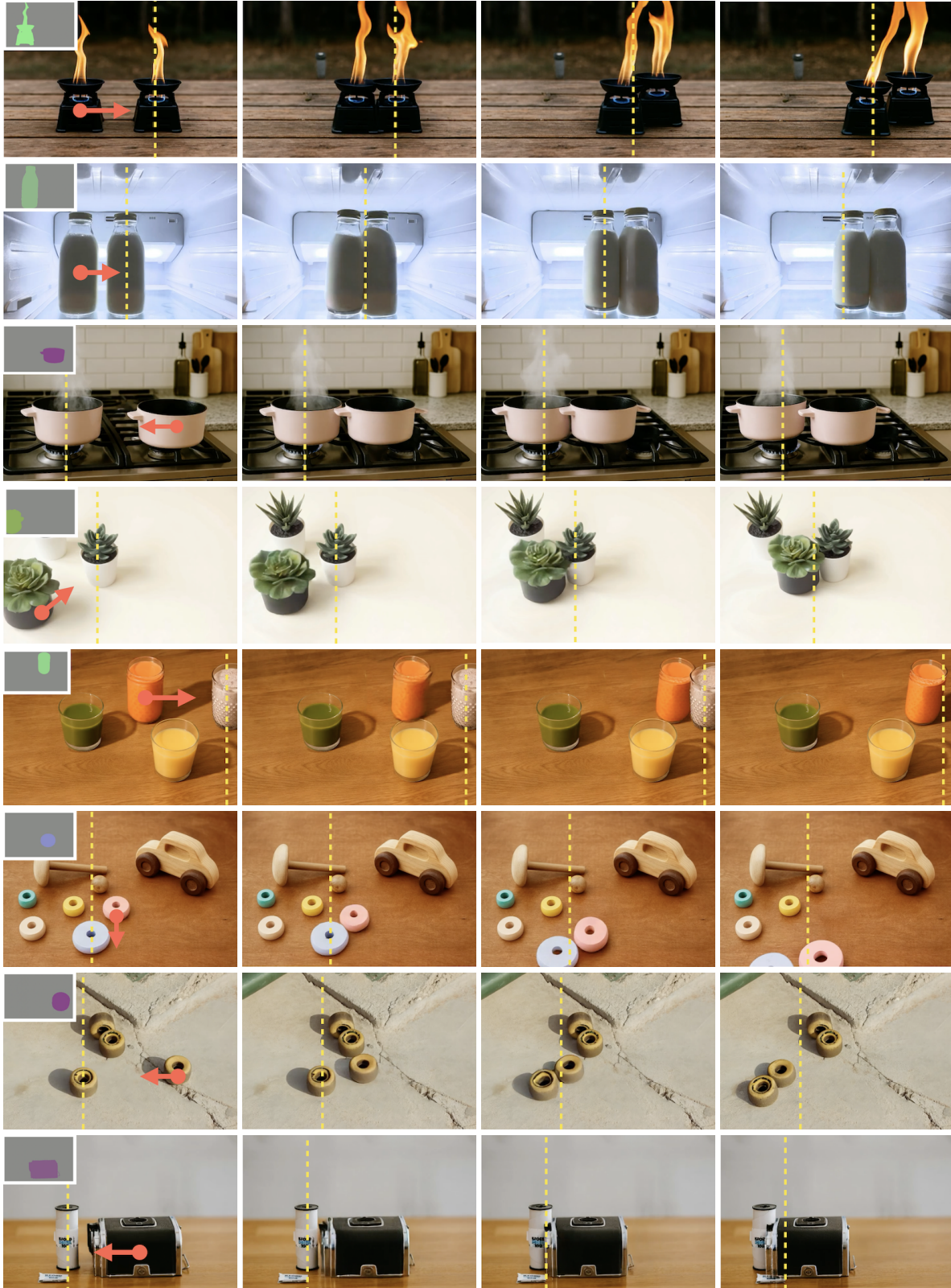


Figure 16. Additional qualitative examples of KineMask.

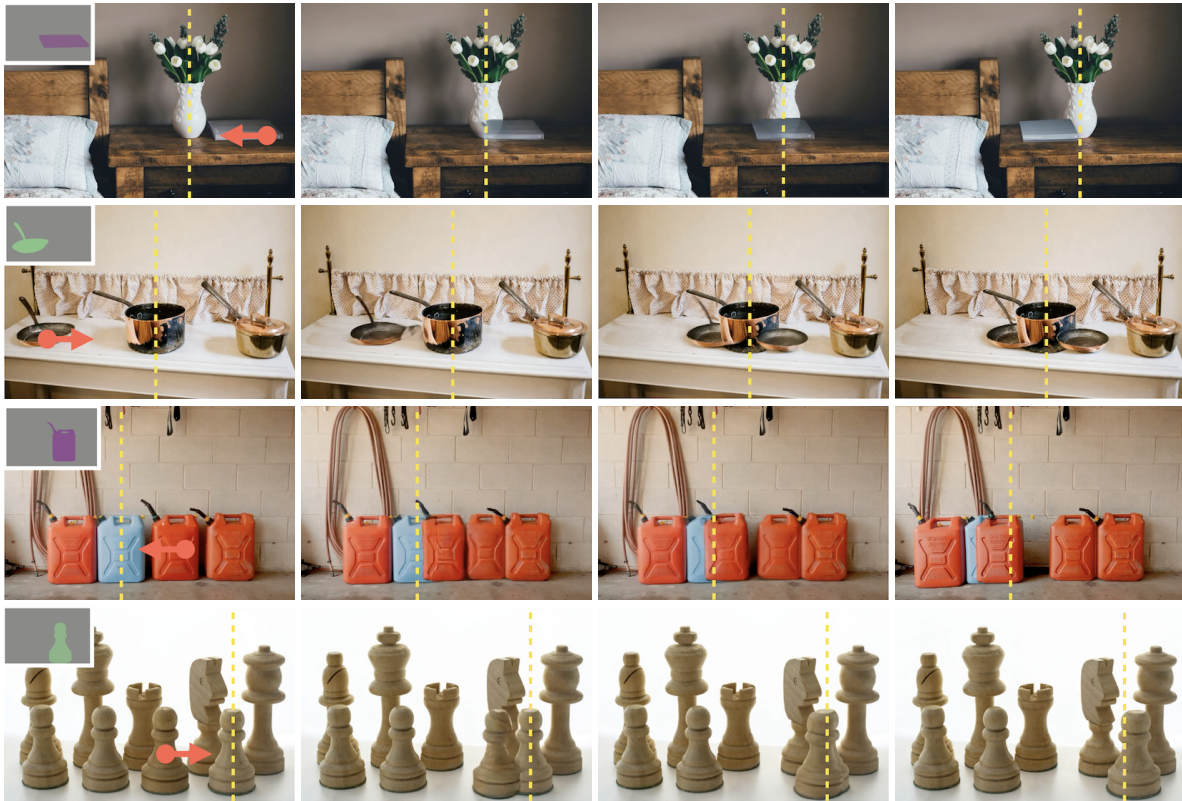


Figure 17. **Failure Cases.** We noticed that KineMasks fails to generate collisions with objects that do not have a considerable height and in ambiguous setups that contain multiple similar objects.